Zirconium Bromide Cluster Chemistry. A New Tunnel Structure in $A_5Zr_6Br_{15}Be$ (A = Rb, Cs)

Ru-Yi Qi and John D. Corbett*

Department of Chemistry, Iowa State University, Ames, Iowa 50011

Received July 7, 1994[⊗]

Reactions in the $ABr-ZrBr_4-Be$ systems (A = Cs, Rb) at ~850 °C yield phases with a new tunnel structure constructed from a $[Zr_6(Be)Br_{12}]Br_{6/3}$ network. Crystal refinements are given for hexagonal $Rb_{5.0(1)}Zr_6Br_{15}Be$ ($P6_322$, $Z = 2$, $a = 13.009(1)$ Å, $c = 12.060(1)$ Å, $R/R_w = 4.4/4.8\%$) and $Cs_{4.60(8)}Zr_6Br_{15}Be$ ($P6_3$, $Z = 2$, $a = 13.105(1)$ Å, $c = 12.156(1)$ Å, $R/R_w = 4.9/3.5\%$). The boride also exists in the rubidium system. The alkali-metal cations all exhibit fractional occupancies, most being located within or on the walls of the tunnels defined by the bridged cluster array, some with only three close bromine neighbors. Some two-site disorder appears in the rubidium structure (and persists in a marginal refinement of it in $P6_3$), while this problem is absent in the cesium compound refinement in the lower symmetry. These characteristics are common in cluster network structures containing larger cations. The formation of 16-e clusters is achieved even with the limited binding of some cations, the cesium salt showing only temperature-independent paramagnetism. This structure type defines a new, fifth type of a $M_6X_{12}X_{6/2}$ network.

Introduction

The remarkable structural and compositional diversity documented for zirconium cluster halides owes its existence to several factors. These originate with the intrinsic stability of $Zr_6X_{12}Z$ cluster units in which the metal octahedron is always edge-bridged by 12 inner halides X^i and, by example, always centered by an interstitial heteroatom Z. The exo positions at each metal vertex evidently must also be bonded to a halide (or other ligand), and this may originate with X^i in other clusters, additional halide that are X^{a-a} bridging between clusters, or solely terminal X^a. Finally, alkali-metal (and possibly other) cations A may be bound within cavities among the halides and thereby alter the electronics and structures. Nearly all of these fall within a general series $A_x(Zr_6X_{12}Z)X_n$. The closed-shell cluster electron counts near 14 or 18 that usually pertain with main group or transition metal Z, respectively, may accordingly be obtained in a given system through appropriate or fortuitous variations among the electronic contributions of Z as well as the values of x and n. Observation of phase stability ultimately also depends on more subtle details: the cluster size, the existence of suitable cavities for A, Zr−Z bond strength, and, often most telling, the relative stability of alternate phases such as ZrZ_x.[1-3]

The zirconium chlorides have afforded the largest variety of structure types with the variables Z = H, Be−N, Mn−Ni as well as $0 \le x, n \le 6$. In contrast, zirconium iodides are to date known only for two families, $Zr_6I_{12}Z$ and $AZr_6I_{14}Z$, that is, only with $n = 0$ or 2, but these also include examples with Z = Al, Si, Ge, or P. We recently completed a comparative examination of the intervening bromides, recognizing that some average of chloride and iodide characteristics might not be very certain because of the particular importance of size variables and matrix effects with both halogens. In fact, this is exactly the case.[4] Although six examples, or close relatives, of chloride stoichiometries and structures are found as bromides, there are also five new structure types, largely unprecedented, illustrating again how subtle are the factors that determine structure and stability in such systems. The present article reports on a new member of the $A_n(Zr_6X_{12}Z)X_{6/2}$ structural series in which X^{a-a} linkages connect all clusters into three-dimensional networks. Four distinctive arrays have already been defined among chlorides, arrangements that are not interconvertable without bond breakages.[5-8] This article reports a fifth type in which a larger number of cations are accommodated in a novel tunnel structure, viz., for $Rb_5Zr_6Br_{15}Be$ and a related cesium example.

Experimental Section

The handling of reactants and products, the reaction techniques in sealed Ta containers, and the characterization procedures, including Guinier powder pattern means, have been described before.[5,9] The beryllium flake and amorphous boron reagents came from Aldrich (three 9's and five 9's, respectively), the zirconium, reactor-grade crystal bar, material was from Ames Laboratory (<500 ppm Hf), and the Br_2 was an A. D. Mackay product (<0.02% Cl_2). The reagent-grade CsBr and RbBr were vacuum sublimed before use.

$ZrBr_4$ was prepared by reaction of the elements in an evacuated and sealed, two-armed fused silica vessel with $Br_2(l)$ at 40−50 °C in one side and the metal strips at 450 °C in the other. The product was sublimed several times over Zr and through a frit while under high vacuum. Powdered Zr (100 mesh) was again obtained via ground ZrH_2 that was dehydrogenated at ≤700 °C in high vacuum. Most reactions were run on a 200−250 mg scale. The identity of any interstitial is established principally through the assurance that its presence is essential to the synthesis of a given structure with specific lattice constants and that a quantitative synthesis, or nearly so, is possible when that component is correctly identified. This also requires careful attention to the delusions possible when yields are low and adventitious impurities serve as interstitials. Yields and dimensions are the best ways to distinguish these. Furthermore, the refined composition of the crystals

[⊗] Abstract published in *Advance ACS Abstracts,* March 1, 1995.

(1) Ziebarth, R. P.; Corbett, J. D. *Acc. Chem. Res.* **1989**, *22*, 256.
(2) Corbett, J. D. In *Modern Perspectives in Inorganic Crystal Chemistry*; Parthé, E., Ed.; Kluwer Academic Publishers: Dordrecht, The Netherlands, 1992; p 27.
(3) Hughbanks, T.; Rosenthal, G.; Corbett, J. D. *J. Am. Chem. Soc.* **1988**, *110*, 1511.
(4) Qi, R.-Y. Ph.D. Dissertation, Iowa State University, 1993.
(5) Ziebarth, R. P.; Corbett, J. D. *J. Am. Chem. Soc.* **1987**, *109*, 4844.
(6) Ziebarth, R. P.; Corbett, J. D. *J. Less-Common Met.* **1988**, *137*, 21.
(7) Ziebarth, R. P.; Corbett, J. D. *J. Am. Chem. Soc.* **1988**, *110*, 1132.
(8) Zhang, J.; Corbett, J. D. *Inorg. Chem.* **1991**, *30*, 431.
(9) Payne, M. W.; Corbett, J. D. *Inorg. Chem.* **1990**, *29*, 2246.

0020-1669/95/1334-1646$09.00/0

Table 1. Diffraction Collection and Refinement Data

	$Rb_{5.0(1)}Zr_6Br_{15}Be$	$Cs_{4.60(8)}Zr_6Br_{15}Be$
fw	2182	2366
space group, Z	$P6_322$ (No. 182), 2	$P6_3$ (No. 173), 2
cell params[a]		
a, Å	13.009(1)	13.105(1)
c, Å	12.060(1)	12.156(1)
V, Å^3; d, g/cm^3	1767.6(4); 4.10(2)	1808.1(4); 4.35(2)
abs coeff (Mo Kα), cm^{-1}	211.4	225.0
no. of indep reflns, var	769, 59	1428, 94
R,[b] %	4.4	4.9
R_w,[c] %	4.8	3.5

[a] Guinier powder data with Si as internal standard, 22 °C, λ = 1.540 562 Å. [b] $R = \sum||F_o| - |F_c||/\sum|F_o|$. [c] $R_w = [\sum w(|F_o| - |F_c|)^2/\sum w(F_o)^2]^{1/2}$, $w = \sigma_F^{-2}$.

studied is the best available provided that a subsequent reaction at that stoichiometry gives a high or, preferably, a single-phase yield according to Guinier data, where the detection limit is 2−5%. Since fractionation of a product mixture is usually not possible in the traditional sense, the direct analysis of a product can only replicate what was loaded.

A powder pattern of this structure type was originally seen in mixtures from reactions of RbBr, $ZrBr_4$, Zr, and Z loaded as either $Rb_4Zr_6Br_{15}B$ or $Rb_4Zr_6Br_{15}Be$ that had been carried out at 830 °C for about 4 weeks. A high yield of the beryllide was later secured from a reaction with the stoichiometry refined. Several reactions subsequently carried out with cesium as the countercation also led to the identification of the nearly isostructural cesium beryllide. A decrease of the Cs reaction content from four to three per cluster increased the cell volume by only 2.8(4) Å^3 (0.15%), suggesting only a small phase breadth. Crystals of the new phases are dark purple. Reaction mixtures containing only about two Rb or Cs per cluster repeatedly yielded different unknown phases. Potassium did not appear to provide either of these structures under any conditions. Magnetic susceptibility data at 3 T were secured on a Quantum Design MPMS SQUID instrument between 6 and ~300 K. The sample under He was held between two silica rods in a specially designed container.[10]

$Rb_5Zr_6Br_{15}Z$ (Z = B, Be). Oscillation as well as zero- and first-layer Weissenberg film studies on a crystal from the $Rb_4Zr_6Br_{15}B$ reaction revealed a hexagonal lattice with $a = b \simeq 12.7$ Å and $c \cong 11.9$ Å that appeared to have a mirror plane perpendicular to c. There were no systematic absences in the a-b nets, and $00l$ absences for odd l suggested space groups $P6_3$, $P6_322$, and $P6_3/m$. This evidence was confirmed by two octants of data from Mo Kα radiation collected on a CAD4 diffractometer up to 55° in 2θ. A reasonable model was obtained in $P6_322$ by direct methods (SHELXS-86[11]), and the observed data were merged with R_{ave} = 4.8% after empirical absorption corrections according to ψ-scan measurements. The apparent Zr and Br positions in the model appeared to define a new type of interlinked 6−15 network. Relatively small peaks in a difference Fourier map after isotropic refinement were reasonable for Rb. One at (0, 0, 0.2) yielded a pair of close positions with a very elongated anisotropic ellipsoid encompassing the two, and one of the Br atoms had a similar behavior as well. The composition was near $Rb_{2.8}Zr_6Br_{15}B$ at R = 7.6%. Lowering the symmetry to $P6_3$ did not solve the problems or further the refinement. Very long exposures of oscillation and Weissenberg photos gave no evidence of any superlattice. The hexagonal lattice constants (Guinier data) for the above phase were a = 12.934(1), c = 11.890(1) Å, and V = 1722.5(4) Å^3, very similar to 12.921(1) Å, 11.888(2) Å, and 1718.9(4) Å^3, respectively, from a $Rb_3Zr_6Br_{15}B$ composition, suggesting the compound is substantially a line phase.

Problems with the apparent disorder in the corresponding beryllide, which contains more cations, are much less serious than those in the boride. Two octants of data collected on the CAD4 to $2\theta = 50°$ yielded the same extinction condition and R_{ave} = 5.0% after a ψ-scan-based absorption correction. Selected data are given in Table 1. The Zr and Br positions from the boride refinement in the same $P6_322$ yielded four cation positions after isotropic refinement of the former. The same Rb1 position as before was farther from the troubling 2-fold axis, and the split peaks refined very close to 50% occupancy each although their ellipsoids were larger than those for the well-ordered cations Rb3 and Rb4 and were elongated along c by ~8:1. Similar behavior was also observed at the Rb2 general position (~1/6, 0, 0) near another 2-fold axis. Fourier maps computed for planes that contain each of these cation pairs (supplementary material) appeared consistent with their assignment as split atoms in relatively large or low-symmetry cavities. The refinement converged well at $R(F)$ = 4.4%, R_w = 4.8%, and the highest peak in the final difference Fourier map, 1.49 e/Å^3, was followed by five more between 1.47 and 1.25 e/Å^3, i.e., background, while the largest negative peak was −1.37 e/Å^3. The parameters are listed in Table 2. The other enantiomer yielded slightly higher residuals. A data set collected at −50 °C gave smaller ellipsoids but no significant changes in order.

Table 2. Positional and Isotropic-Equivalent Thermal Parameters for $Rb_{5.0(1)}Zr_6Br_{15}Be$ ($P6_322$)

atom	position	x	y	z	B_{eq},[a] Å^2
Zr	12i	0.5184(2)	0.3353(2)	0.1359(1)	1.43(6)
Br1	6g	0.6713(3)	0	0	2.3(1)
Br2	12i	0.1669(2)	0.4966(2)	0.0088(2)	2.15(8)
Br3	6h	0.8353(2)	2x	1/4	2.5(2)
Br4	6h	0.4969(2)	2x	1/4	2.0(2)
Be	2d	2/3	1/3	1/4	1(1)
Rb1[b]	4e	0	0	0.179(2)	12(1)
Rb2[b]	12i	0.166(1)	−0.028(2)	0.054(1)	13(2)
Rb3[b]	6h	0.1575(4)	2x	1/4	6.0(5)
Rb4[b]	2c	1/3	2/3	1/4	2.5(5)

[a] $B_{eq} = (8\pi^2/3)\sum_i\sum_j U_{ij}a_i^*a_j^*\vec{a}_i^*\vec{a}_j$. [b] Occupancies: Rb1, 49(1)%; Rb2, 31(1)%; Rb3, 64(1)%; Rb4, 29(1)%.

Comparison with results for a very similar $Cs_{4.6}Zr_6Br_{18}Be$ (below), which refined well in the lower Laue group $P6_3$, and a reviewer's pertinent comments, prompted an examination of twinning prospects with the aid of SHELXL-93.[11] However, rubidium F_o^2 data and atom parameters from either the cesium result or other subsets of the refined disorder would not refine at all as a twin generated by the equivalent of the 2-fold axes in $P6_322$, even for the problem-free Zr_6Br_{15} portion of the structure. The structure was also refined in $P6_322$ with SHELXL, with only small differences. The ellipsoids were generally a little smaller than reported, the Rb occupancies were nearly identical, and appreciable residuals (~0.2 Rb) remained at 0, 0, 0.25 (compare the Cs salt) and near Rb2 (R_1 = 0.048, wR_2 (F^2) = 0.128). Further examination of the problem in $P6_3$ with an untwinned model suggested that the structure really is at least partially disordered. With care, the rubidium structure could be refined to $R_1(F)$ = 5.6%, wR_2 = 0.173, but Rb2 (and U_{33} for some other Rb atoms) became very large when U_{ij} terms for the former were released. In general, the U_{33} and, to a lesser degree, z parameters were not well constrained or defined. In comparison with the partly disordered rubidium structure reported here for $P6_322$ and the successful Cs refinement in $P6_3$ (Tables 2 and 3; Results and Discussion), this $P6_3$ rubidium model still contains the pair of Rb1 atoms seen with higher symmetry, somewhat further apart. One of these had a normal U_{33} and the other was large, as before, and a third atom appeared between them near 0, 0, 0.25 and ~30% occupancy, as found alone with Cs (Table 3). On the other hand, only one of the sets derived from Rb2 in the 12i position (Table 2) appeared, although again large and, as noted above, not completely refinable. Rb3 and Rb4 were similar to before. The ellipsoid sizes and position occupancies were generally smaller than before (except for Rb2), indicating the characteristics of it are evidently intrinsic. The largest residual was ~3.9 e/Å^3.

$Cs_{4.6}Zr_6Br_{18}Be$. The crystal used came from a reaction loaded as $Cs_4Zr_6Br_{15}Be$ and run at 830 °C for 6 weeks. (A rhombohedral $Cs_{3.4}Zr_6Br_{15}B$ forms with boron.[4]) A hemisphere of data was collected on the CAD4 diffractometer. The positional parameters refined for $Rb_5Zr_6Br_{15}Be$ were utilized in an initial model after ψ-scan-based corrections. This resulted in an electron density around Cs1 that was elongated along c, the tunnel direction, as observed for Rb1, but there was no evidence for splitting, and the center of the electron density lay right on the special position (0, 0, 1/4). However, Br4 on a 2-fold

(10) Sevov, S. C.; Corbett, J. D. *Inorg. Chem.* **1992**, *31*, 1895.
(11) Sheldrick, G. M. SHELXS-86 and SHELXL-93, Universität Göttingen, Germany, 1986 and 1993.

Table 3. Positional and Thermal Parameters for $Cs_{4.60(8)}Zr_6Br_{15}Be$ ($P6_3$)

atom	position	x	y	z	B_{eq}[a] Å^2
Zr1	6*c*	0.5196(2)	0.1844(2)	0.3633	1.06(8)
Zr2	6*c*	0.5196(2)	0.3351(2)	0.1365(2)	1.05(8)
Br1	6*c*	0.6667(2)	−0.0002(2)	−0.0022(7)	1.82(8)
Br21	6*c*	0.1672(3)	0.4972(2)	−0.0069(4)	1.6(1)
Br22	6*c*	0.1674(2)	0.6698(2)	0.4948(4)	1.8(1)
Br3	6*c*	0.8336(3)	0.6667(2)	0.2525(5)	1.76(8)
Br4	6*c*	0.4982(3)	0.0038(2)	0.2523(4)	1.26(9)
Be	2*b*	$^2/_3$	$^1/_3$	0.228(4)	2(1)
Cs1[b]	2*a*	0	0	0.245(1)	10.7(5)
Cs21[b]	6*c*	0.185(1)	0.031(2)	−0.034(1)	5.6(5)
Cs22[b]	6*c*	0.153(1)	−0.021(1)	0.029(1)	7.6(4)
Cs3[b]	6*c*	0.1616(2)	0.3229(3)	0.2525(6)	4.0(1)
Cs4[b]	2*b*	$^1/_3$	$^2/_3$	0.248(1)	4.2(2)

[a] $B_{eq} = (8\pi^2/3)\sum_i\sum_j U_{ij}a_i^*a_j\vec{a}_i\vec{a}_j$. [b] Occupancies: Cs1, 60.0(9)%; Cs21, 18(1)%; Cs22, 27(1)%; Cs3, 76.1(3) %; Cs4, 36.3(6)%.

axis had a peculiar thermal ellipsoid after anisotropic refinement, and the space group without these axes, $P6_3$, seemed a better choice. This afforded a distinctly better solution, for not only could Br4 be described by a small and fairly spherical distribution, but also the R and R_w values at convergence were lowered significantly, from 6.0/4.5% to 4.9/3.5%. In $P6_322$, Cs2 behaved similar to the split Rb2, but in $P6_3$ the two sites could be refined independently and gave different occupancies [18(1)% and 27(1)%], apparently further support for the correctness of the lower symmetry space group. However, the substantial overlap of these distributions when refined anisotropically meant the refined positions lay between the peaks observed in both Fourier and difference Fourier maps. Therefore, these two positions were isotropically refined. (Fourier maps of the Cs1 and Cs2 regions are also given in the supplementary material.) The other enantiomer was discarded because of its higher residuals (5.8% and 4.3%). The final positional and isotropic-equivalent displacement parameters are listed in Table 3 in the setting comparable to that in the rubidium phase description. The final difference Fourier map was essentially flat, with a 1.8 e/Å^3 maximum 1.15 Å from Br3. The very light Be atom persistently refined to an illogical, off-center position within the cluster (by 0.27 Å, 5.5σ), probably the result of parameter coupling, but the distances from the usual midpoint site were typical for Zr−Be. The more accurate lattice constants from Guinier data were used for distance calculations for both structures.

Additional data collection and refinement information, the anisotropic displacement parameters, and Fourier maps of A1 and A2 regions in both structures are contained in the supplementary material. These and the F_o/F_c data may also be obtained from J.D.C.

Results and Discussion

The $Rb_5Zr_6Br_{15}Be$ Structure. The principal, and striking, feature of this new type of M_6X_{15} structure is the existence of large tunnels generated by clusters interbridged at all vertices by $Br1^{a\text{-}a}$ or, conversely, a tunnel structure propped open by cations therein, namely the A1, A2, and A3 ions. The first two exhibit some disorder problems in this phase, evidently because of their small numbers of bromide neighbors and the low symmetry. Figure 1a gives an overview of the tunnel along [001]. (Note that all 12 of the inner edge-bridging bromines about each cluster have been omitted for clarity.) A 6_3 axis runs down the center of each tunnel while Be at each cluster center lies at the intersection of 3-fold and three 2-fold axes that are perpendicular to and in the plane of the page, respectively. As shown in Figure 1b, each cluster is bridged to three clusters above and three below that are eclipsed, that is, in an hcp packing arrangement, the bridges in the two halves bending in opposite ways. As in other cases,[12,13] the network can alternatively be described in terms of 12 close-packed layers

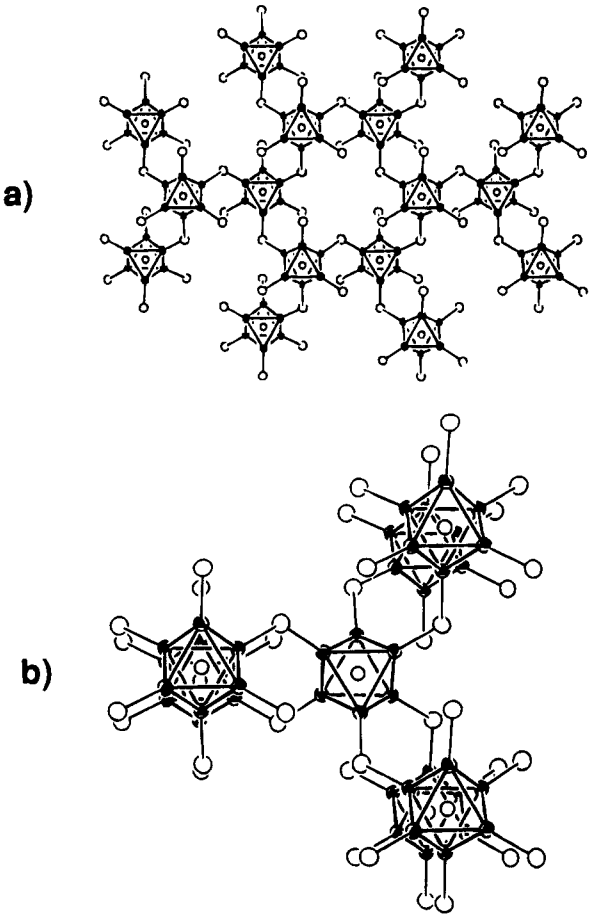

Figure 1. [001] views of $Rb_5Zr_6Br_{15}Be$: (a) the cluster network and the tunnels thereby defined; (b) the local environment around each cluster unit at the junction of three tunnels. Both the rubidium atoms and the 12 inner bromine atoms about each cluster are not shown.

of atoms normal to c that are sequenced ...ABCB... or $(hc)_2$. Layers A and C contain 9 Br and 3 A cations while layer B is composed of 6 Br, 5 A, and 1 Be. Zirconium lies between them in groups of three in those "octahedral" sites where each has 5 Br and 1Be neighbors.

The means by which the Rb^+ countercations are accommodated are one of the unusual aspects of the structure and will be described separately. Figure 2a is a more detailed picture of the distribution of just the Rb1, Rb2, and Rb3 cations within the tunnels defined by the $(Zr_6Be)-Br1^{a\text{-}a}$ network, the other Br^i atoms being omitted. The Br^i atoms in the tunnels that provide most of the cations' nearest neighbors have been added in Figure 2b for the closer layer of cations to illustrate more clearly how the tunnel is constructed and filled. The first parts of the following discussion will be clearer if the upper figure is consulted.

Each of three cation sites presents an unusual situation. As shown in Figure 3, pairs of the axial Rb1 each show an very elongated distribution along the tunnel ($U_{33}/U_{11} \sim 8$), and the 49(1)% occupancy of each is presumably correlated to avoid an otherwise short separation of 1.72 Å (Table 4). The split Rb1 pair and the ellipsoid behavior presumably originate with its nearest neighbor distribution, namely, only three Br3 atoms around the waist plus the effect of a neighboring pair of Rb2 atoms (below). Likewise Rb2 at 31(1)% occupancy is distributed over a pair of close sites in this space group, again evidently because of the low-symmetry environment. Figure 4 shows how one Rb2 site has three reasonably placed neighbors at $\bar{d}$ = 3.41 Å plus three more at $\bar{d}$ = 3.99 Å, the latter being the close neighbors of the other Rb2 component related by a vertical

(12) Imoto, H.; Corbett, J. D.; Cisar, A. J. *Inorg. Chem.* **1981**, *20*, 145.
(13) Zhang, J.; Corbett, J. D. *Inorg. Chem.* **1993**, *32*, 1566.

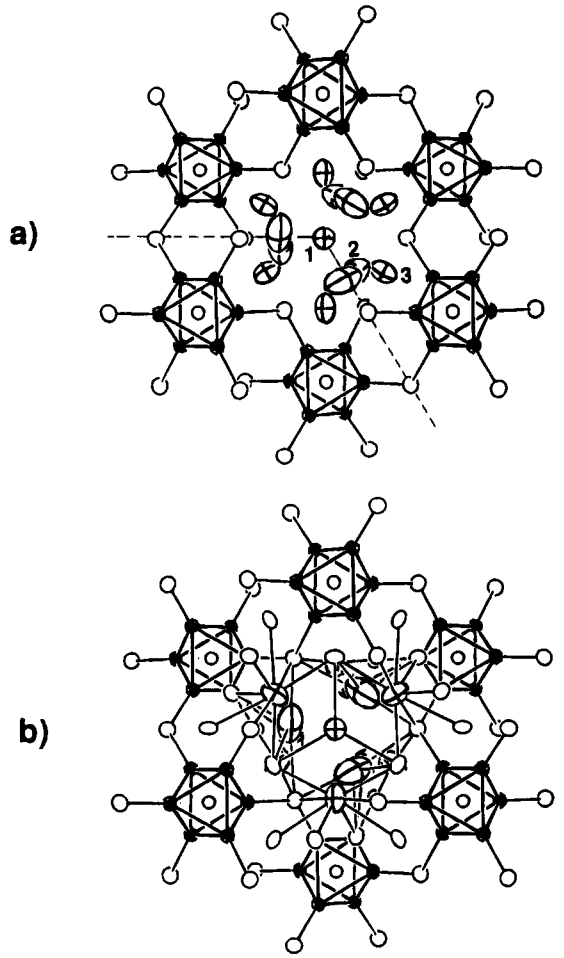

Figure 2. [001] view of the tunnel structure of $Rb_5Zr_6Br_{15}Be$ (6_3 symmetry, with $c/2$ shown): (a) a short section of the tunnel created by six clusters and the Rb1, Rb2, Rb3 cations within (crossed, 90% ellipsoids), all Br^i atoms omitted for clarity; (b) the above view with the tunnel better defined by all the bromine atoms (open ellipsoids) that are neighbors to the nearest rubidium atoms (50% probability).

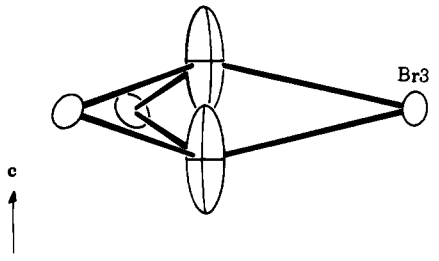

Figure 3. Local environment of Rb1 in $Rb_5Zr_6Br_{15}Be$, D_3 symmetry. Each of the Rb1 pair at 50% occupancy is at a mean refined distance of 3.81 Å from Br3. The sum of CN6 crystal radii is 3.48 Å.

2-fold axis along x, 0, 0. (The two are separable in the Cs salt.) The Figure 4 view is related to that in Figure 2a by a 90° rotation; the pair of partially eclipsed Rb2 atoms in Figure 2 at $z = \pm 0.054$ have the pair of bridging Br1 at (0.33, 0, $\pm 1/2$) as neighbors. Rb2 is thus presented with a fairly elongated cavity, and in this model it is bonded ~31% of the time on each of the opposite faces. This disorder may in fact be some of the reason for the Rb1 disorder (Figure 3) as the Rb2−Rb1 (midpoint) separation is 3.34 Å; Rb3 may also contribute to the former. One plausible explanation of the foregoing distributions could be merohedral twinning of a $P6_3$ structure about a 2-fold axis normal to c (as noted in Figure 2), but such a model (based on the Cs structure below) could not be refined (Experimental Section). Thus, the structure appears to exhibit true disorder

Table 4. Important Distances (Å) and Angles (deg) in $Rb_{5.0(1)}Zr_6Br_{15}Be$

Zr−Zr	×2	3.363(3)	Rb1−Rb1[a]	×1	1.72(4)[b]
	×1	3.345(4)	Rb1−Rb2	×3	2.80(2)[b]
	×1	3.390(4)	Rb1−Rb2	×3	3.67(2)
$\bar{d}$		3.365	Rb1−Rb3	×3	3.652(9)
			Rb2−Rb2	×1	1.44(4)[b]
Zr−Be	×1	2.380(2)	Rb2−Rb3	×1	2.87(2)
Zr−Br2[i]	×2	2.703(3)	Br1−Br2[c]	×2	3.717(3)
Zr−Br2	×2	2.722(3)	Br1−Br3	×2	3.696(1)
Zr−Br3[i]	×2	2.722(4)	Br1−Br4	×2	3.750(2)
Zr−Br4[i]	×2	2.710(4)	Br2−Br2	×1	3.766(5)
			Br2−Br2	×2	3.791(3)
Zr−Br1[a-a]	×1	2.928(2)	Br2−Br3	×1	3.797(3)
			Br2−Br4	×1	3.608(3)
Rb1−Br3	×3	3.808(7)			
			Zr−Zr−Zr	×1	60.00
Rb2−Br1	×1	3.46(3)		×1	59.39(8)
Rb2−Br2	×1	3.46(1)		×1	59.91(6)
Rb2−Br3	×1	3.32(2)		×1	89.61(5)
$\bar{d}$		3.41	Zr−Br1−Zr	×1	128.3(1)
Rb3−Br1	×2	3.699(1)	Br2−Zr−Br3	×2	167.4(1)
Rb3−Br2	×2	3.711(5)	Br2−Zr−Br4	×2	165.8(1)
Rb3−Br3	×2	3.633(3)			
Rb3−Br4	×2	3.831(4)			
$\bar{d}$		3.718			
Rb4−Br2	×6	3.641(2)			
Rb4−Br4	×3	3.686(4)			
$\bar{d}$		3.656			

[a] d(Rb−Rb) < 3.70 Å. [b] Distances between nearest components of twin, fractionally occupied sites that are presumably avoided by correlations. [c] d(Br−Br) ≤ 3.80 Å.

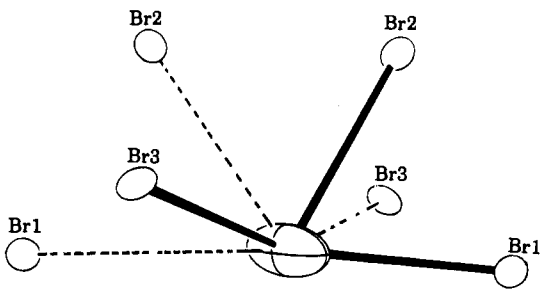

Figure 4. Local environment about one of the two Rb2 sites (31% occupied) in $Rb_5Zr_6Br_{15}Be$, with nearest neighbors at 3.32−3.46 Å marked by heavy lines. The c axis runs horizontally, and a vertical 2-fold axis (x, 0, 0, etc.) relates the three pairs of bromine atoms and the other Rb2 site.

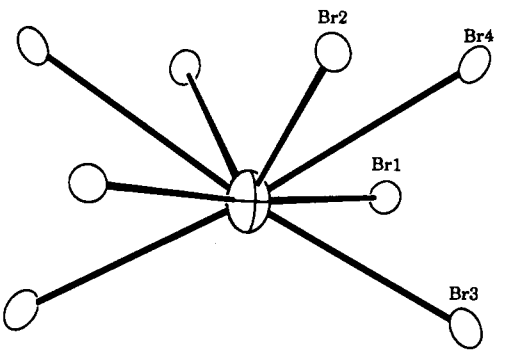

Figure 5. Local environment of Rb3 in $Rb_5Zr_6Br_{15}Be$ (C_2 symmetry) with eight Br neighbors (50% probability). The c axis is approximately horizontal and parallel to the page, while a 2-fold axis lies vertical.

of some cations. Complete refinement of the structure in $P6_3$ to eliminate at least the Rb2 pairwise distributions was not possible, although it may be the correct description.

The best situated cation inside the tunnel is Rb3, which lies closest to the tunnel wall at a point of C_2 symmetry with eight Br atoms around it, Figure 5. The average Rb3−Br distance,

3.72 Å, is nonetheless 0.15 Å longer than the sum of crystal radii, 3.57 Å,[14] and the Rb3 occupancy is 64(1)%. Only the Rb4 cation lies outside the tunnel at a point of D_3 symmetry between clusters with the same projection (AA or BB). It has 9 neighboring Br atoms at an average distance of 3.656 Å, only *ca.* 0.07 Å more than the crystal radius sum. The refined occupancy is 29(1)%, making Rb4 only about 6% of the total cation content in $Rb_{5.0(1)}Zr_6Br_{15}Be$. The considerable number of surplus cation sites that are energetically similar is one of the notable features of this structure.

There is nothing particularly remarkable about the Zr_6Br_{12}-Be cluster itself. The Zr−Be distance, 2.380(2) Å, is close to the average in $Rb_3Zr_6Br_{15}Be$, 2.376 Å (slightly tetragonally compressed).[4] This is reasonably larger than the 2.333 Å in $K_3Zr_6Cl_{15}Be$ and others[2,7] since a small matrix effect is probably operable around the present cluster because of $Br^i\cdots Br^i$ contacts as short as 3.61 Å.

$Cs_{4.6}Zr_6Br_{15}Be$. As described in the Experimental Section, the refinement of the $Cs_{4.6}Zr_6Cl_{15}Be$ structure in the lower symmetry space group $P6_3$ provides a distinctly better solution that has no split atom problems. This reduction means the 12-fold sites occupied in the above salt by Zr, Br2, and Rb2, the last of which was already split into a like pair by a nearby 2-fold axis, are now divided into independent 6-fold sets. The Zr−Br framework is essentially the same as that of $Rb_5Zr_6Br_{15}Be$, and the differences are on Cs1 and Cs2 sites. The thermal displacement of Cs1 along the tunnel direction is still appreciable ($U_{33}/U_{11} \sim 9$), but it is not split as was Rb1. The three Br3 atoms around its waist are 3.783(2) Å away (Table 5) compared with a six-coordinate radius sum of 3.63 Å,[14] and the Cs1 occupancy is refined to be 60.0(9)%. An independent pair Cs21 and Cs22, which correspond to the split Rb2, can be isotropically refined about 1.0 Å apart. Their x parameters differ from equivalency by 7.8σ, and their refined occupancies, 18(1)% and 27(1)%, respectively, differ by 6.4σ. The atoms are still effectively three-coordinate (compare Figure 4), but the average Cs22−Br distance, 3.63 Å, is 0.11 Å greater than that around the more populated Cs21 site. (Some coupling of the refined results may be present, of course.)

The environment of Cs3 now shows some significant deviations from C_2 symmetry (Table 5). The average Cs−Br distance is 3.75 Å, only slightly greater than the eight-coordinate sum, 3.70 Å. The last Cs4 site between clusters still has D_3 symmetry and the average Cs4−Br distance, 3.71 Å, is nearly ideal for a nine-coordinate Cs^+ (3.74 Å). In contrast, all the cation sites in $Rb_5Zr_6Br_{15}Be$ appear relatively too large for Rb^+. The refined occupancies of all the Cs sites yield an overall composition of $Cs_{4.60(8)}Zr_6Br_{15}Be$, the only decreases from those in $Rb_5Zr_6Br_{15}$-Be appearing to occur at the less well coordinated A1 and A2 sites. Considering the relatively large errors on the refined cation occupancies, the cesium derivative is still virtually a 16-e cluster phase. The cluster core (Zr_6Be) is substantially the same as before. The small increase in lattice constants found with the heavier cation parallel a 2° opening of the bridging Zr−Br1−Zr angles, an increase in the Zr2−$Br1^{a-a}$ distance of 0.03 Å, and 0.05 and 0.09 Å increases of the shortest 3.61 Å Br2···Br4 contacts in the rubidium phase.

Magnetic susceptibility measurements were performed on the nearly single-phase product of a reaction loaded as $Cs_5Zr_6Br_{15}$-Be. The magnetic susceptibility of this sample (supplementary material) is, surprisingly, essentially independent of temperature above ~70 K, $4.68(1) \times 10^{-4}$ emu mol^{-1} after diamagnetic core corrections. Since a phase with this structure is presumably a semiconductor, this must mean there are no localized unpaired electrons and that the compound contains a 16-electron cluster with the expected a_{2u}^2 HOMO.[1] Such temperature-independent paramagnetism is presumably caused by mixing of wave functions for excited, paramagnetic states with those of the ground state in the presence of the magnetic field, the so-called Van Vleck paramagnetism. We have observed a comparable χ_{TIP} value for the paramagnetic $Cs_{3.4}Zr_6Br_{15}B$,[4] and similar values are well-known for many $(M_6Cl_{12})Cl_n$ cluster compounds for M = Nb and Ta.[15]

Table 5. Important Distances (Å) and Angles (deg) in $Cs_{4.60(8)}Zr_6Br_{15}Be$

Zr1−Zr1	×2	3.359(4)	Cs3−Br1	×1	3.701(6)
Zr1−Zr2	×1	3.350(2)	Cs3−Br1	×1	3.789(6)
Zr1−Zr2	×1	3.391(2)	Cs3−Br21	×1	3.738(6)
Zr2−Zr2	×2	3.359(4)	Cs3−Br22	×1	3.707(6)
d		3.365	Cs3−Br3	×1	3.721(6)
			Cs3−Br3	×1	3.729(6)
Zr1−Be	×1	2.54(3)	Cs3−Br4	×1	3.821(6)
Zr2−Be	×1	2.24(3)	Cs3−Br4	×1	3.826(6)
d		2.39	*d*		3.754
Zr1−$Br21^i$	×1	2.709(4)	Cs4−Br21	×3	3.67(1)
Zr1−Br21		2.725(4)	Cs4−Br22	×3	3.72(1)
Zr1−$Br3^i$	×1	2.696(4)	Cs4−Br4	×3	3.740(2)
Zr1−$Br4^i$	×1	2.700(4)	*d*		3.71
Zr2−$Br22^i$	×1	2.693(4)			
Zr2−$Br22^i$	×1	2.709(4)	Cs1−$Cs21^a$	×3	3.50(2)
Zr2−$Br3^i$	×1	2.725(5)	Cs1−Cs22	×3	3.40(2)
Zr2−$Br4^i$	×1	2.730(4)	Cs3−Cs21	×1	3.13(2)
			Cs3−Cs22	×1	3.31(2)
Zr1−$Br1^{a-a}$	×1	2.927(5)	Cs21−Cs22	×1	0.98(1)[b]
Zr2−$Br1^{a-a}$	×1	2.960(5)	Cs21−Cs22	×1	3.56(1)
Cs1−Br3	×3	3.783(2)			
			Zr1−Zr1−Zr1	×1	60.00
Cs21−Br1	×3	3.45(2)	Zr1−Zr1−Zr2	×1	90.36(7)
Cs21−Br22	×1	3.58(2)	Zr1−Zr1−Zr2	×1	59.51(7)
Cs21−Br3	×1	3.59(2)	Zr1−Br1−Zr2	×1	130.4(1)
d	×1	3.54	Zr1−Br1−Br3	×2	167.0(2)
Cs22−Br3	×1	3.56(1)	Br21−Zr1−Br4	×2	165.3(1)
Cs22−Br3	×1	3.64(1)	Br22−Zr2−Br3	×2	168.1(2)
Cs22−Br21	×1	3.68(1)	Br22−Zr2−Br4	×2	166.3(1)
d		3.63			

[a] d(Cs−Cs) < 3.65 Å. [b] Between split positions of Cs2.

A remarkable feature of these two new compounds, the rubidium salt most clearly, is that they are unusually well reduced, with close to 16 cluster electrons. Both may be obtained in high yield. Although 14 electrons are customary for ideal M_6X_{12} clusters, centered or not, the formation of anomalous 16-e clusters has been found to correlate well with the matrix effects encountered most often with smaller M, smaller Z, or larger X.[16] Basically, closed-shell $X^i\cdots X^i$ repulsions about the cluster are increased by some or all of these size changes, and this causes the metal vertices, largely fixed by M−M and M−Z (if any) bonding, to lie inside the faces of the cube defined by the 12 X^i. This in turn lowers the energy of what is the a_{2u} LUMO in the 14-e case (through loss of π^* M−X^i interactions) sufficiently that further reduction is possible, as in many familiar $(Nb,Ta)_6X_{12}$ compounds as well as for $Zr_6I_{12}Z$ type examples. Useful qualitative comparisons of the effect are found in the deviation of the *trans*-X^i−M−X^i angles in those faces from 180°. The 165−168° values in the present structures are consistent with the 16-e option. Of course, network and Zr−Be bonding and cation accommodation are other factors.

A structure feature of these new phases is the need (or opportunity) to bind additional cations (or *vice versa*) in order to achieve the 16-e $Zr_6Br_{15}Be^{5-}$ clusters, and this is presumably

(14) Shannon, R. D. *Acta Crystallogr.* **1976**, *A32*, 751.

(15) Converse, J. G.; McCarley, R. E. *Inorg. Chem.* **1970**, *9*, 1361.

(16) Ziebarth, R. P.; Corbett, J. D. *J. Am. Chem. Soc.* **1989**, *111*, 3272.

Table 6. Classification of $(M_6X_{12})X_{6/2}$ Structure Types[7]

structure type	space group	X^{a-a} bridge angularity, %		criteria		examples
		linear	bent	ring size[a]	no. of FBS[b] clusters so linked	
Nb_6F_{15}	*Im3m*	100	0	4	4	$Zr_6Cl_{15}Co$, $Re_6S_7Br_4$[c]
$K_2Zr_6Cl_{15}B$	*Cccm*	33	67	4	2, 3	$K_3Zr_6Cl_{15}Be$, $Ba_2Re_6S_{11}$[d]
$CsNb_6Cl_{15}$	*Pmma*	17	83	3	0	$KZr_6Cl_{15}C$, $CsZr_6Cl_{15}C$
Ta_6Cl_{15}	*Ia3d*	0	100	4	2	$Zr_6Cl_{15}N$, $Na_{0.5}Zr_6Cl_{15}C$
$Rb_5Zr_6Br_{15}Be$[e]	$P\bar{6}_322$	0	100	4	3	$Cs_{4.6}Zr_6Br_{15}Be$[e]
$Cs_3Zr_7Cl_{20}Mn$[f]	$R\bar{3}c$	0	100	4	4	$Cs_3Zr_6Br_{15}C$[g]

[a] y in $(-Zr_6-X^{a-a}-)_y$. [b] First bonding sphere (FBS) to a central cluster. [c] Perrin, A.; Leduc, L.; Sergent, M. *Eur. J. Solid State Chem.* **1991**, *28*, 919. [d] Bronger, W.; Missen, H.-J. *J. Less-Common Met.* **1982**, *83*, 29. [e] This work. [f] Reference 17. [g] Reference 18.

less restrictive with relatively large cations. Many other examples among cluster network compounds suggest that the intranetwork bonding arrangement is the most demanding, as determined in major part by the excess halogen beyond $12X^i$, while the larger countercations appear to have the least to say about the ideality or suitability of their nearest neighbor environments or, conversely, to exhibit the more unusual, even troubling, structural features.[1,2,5,7,16] In $Rb_5Zr_6Br_{15}Be$ we have 10 rubidium atoms per cell distributed over 24 sites of four different types, that is, with a 42% average occupancy. The surprising accommodation of such relatively naked and unscreened cations with fractional, and presumably correlated, occupancies seen here bespeaks of a notable stability for the network structure with the better bonded A3 and A4 cations. Ready ion exchange within this lattice would seem likely, although the hydrolytic and oxidative sensitivity of the host will require extra care.

Structural Comparisons among 6−15 Structures. Earlier investigations have provided about 25 $[Zr_6(Z)Cl_{12}]Cl_{6/2}$ phases for which the connectivity into three-dimensional networks can be classified into four distinctive structure types. These are distinguished according to (a) the angularity at the $Zr_6-Cl^{a-a}-Zr_6$ bridges (bent or linear), (b) the size (y) of the smallest rings $(-Zr_6-Cl^{a-a}-)_y$ in the structure, and (c) linkage characteristics among the six first neighbor clusters about a central cluster (first bonding sphere, FBS), that is, to how many other FBS clusters each is linked. These distinctive types cannot be interconverted by rotations, only by breaking and rearranging the Cl^{a-a} connections.[7]

Table 6 lists these characteristics for the four types previously known, namely, those originally defined by the Nb_6F_{15}, $K_2Zr_6Cl_{15}B$, $CsNb_6Cl_{15}$, and Ta_6Cl_{15} structure types, the new example afforded by $Rb_5Zr_6Br_{15}Be$, and another new member in $Cs_3(ZrCl_5)Zr_6Cl_{15}Mn$.[17] The last derives from the Nb_6F_{15} structure, which consists of two interpenetrating but not interconnected cubic arrays of clusters with linear bridges; here the primitive cubic substructure with the $M_6X_{12}X_{6/2}$ connectivity is filled with cations and the $ZrCl_5^-$ anion in what amounts to a stuffed rhombohedral perovskite. Only a few additional members of each family are also given in the table, including some recently defined for face-capped rhenium clusters $[(Re_6X_8)X_{6/2}]$. There are also further examples with distorted versions of these high-symmetry parents.[7]

The ring size and FBS connections for $Rb_5Zr_6Br_{15}Be$ can be verified with the simplified version of the structure connectivity shown in Figure 6 in which the larger spheres represent $Zr_6Br_{12}Be$ clusters and the smaller ones, the Br^{a-a} bridges. The smallest rings all involve four clusters (see also Figure 2). Each numbered FBS cluster about the central (solid) unit can also be seen to be interconnected to three others via the striped, second-sphere clusters. (In each case, there are actually two paths for one of the three connections—see 1−4, for example.)

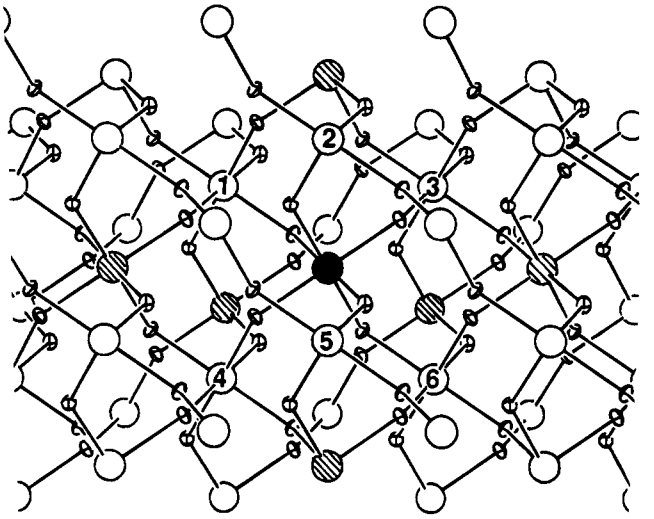

Figure 6. Schematic representation of the cluster connectivity in the $Rb_5Zr_6Br_{15}Be$ lattice with large spheres and small ellipsoids representing $Zr_6(Be)Br_{12}$ and Br^{a-a}, respectively ([010] view, c vertical). A central $Zr_6Br^i_{12}Be$ cluster (solid), the clusters in the first bonding sphere (FBS) numbered 1−6, and the clusters that interconnect FBS members (striped) are marked. Each FBS cluster is connected to three others via four striped clusters.

Finally, the delicate role that the number of cations plays in determining the particular structure is well demonstrated in the systems reported here, where somewhat fewer cations and, sometimes, a small change in Z give a different 6−15 example. In comparison with the present $Rb_5Zr_6B_{15}Be$ and the substantially isostructural $Rb_{\sim 4}Zr_6Br_{15}B$, less rubidium alone gives $Rb_3Zr_6Br_{15}Be$ (with 14 e) in a derivative of the $K_2Zr_6Cl_{15}B$ structure. With cesium, $Cs_{3.4}Zr_6Br_{15}B$ and $Cs_3Zr_6Br_{15}C$ both exhibit a collapsed version of a single Nb_6F_{15} array noted above.[18]

Acknowledgment. This research was supported by the National Science Foundation, Solid State Chemistry, via Grants DMR-8902954 and -9207361 and was carried out in the facilities of Ames Laboratory, U.S. Department of Energy.

Supplementary Material Available: Tables of data collection and refinement details and the anisotropic displacement parameters, Fourier maps of the A1 and A2 regions in both structures, and a plot of the magnetic data for the cesium salt (7 pages). Ordering information is given on any current masthead page.

IC940779B

(17) Zhang, J.; Qi, R.-Y.; Corbett, J. D. *Inorg. Chem.* **1995**, *34*, 1652.

(18) Qi, R.-Y.; Corbett, J. D. *Inorg. Chem.* **1995**, *34*, 1657.